A Broadside-Scanning Half-Mode Substrate Integrated Waveguide Periodic Leaky-Wave Antenna

Robert Henry, *Student Member, IEEE*, and Michal Okoniewski, *Fellow, IEEE*

***Abstract*—A detailed study of a half-mode substrate integrated waveguide (SIW)-fed periodic leaky-wave antenna (LWA) with broadside scanning enabled is presented. Design techniques are outlined. Previously presented simulations have been improved with an enhanced structure model that incorporates substrate anisotropy. Additional theory has been applied to the analysis of the antenna to further validate its leaky-wave operation, and extra prototypes have been characterized for comparison to original measurements and simulations. The prototype antenna displayed a 32% impedance bandwidth within which a 10-dB gain over an 86° scan range (including broadside) was observed such that its radiation performance appears to be comparable to some of the newly popular SIW-based composite right/left-handed leaky-wave antennas.**

***Index Terms*—Leaky-wave antenna, substrate integrated waveguide, traveling wave array.**

I. Introduction

SUBSTRATE integrated waveguide (SIW) has been popularly used in millimeter (mm)-wave frequency applications due to its efficient transmission properties at these frequencies [1], [2]. With the increasing use of SIW comes a need for a variety of SIW-compatible components including antennas. As a result, a new half-mode SIW (HMSIW) periodic leaky-wave antenna (LWA) with broadside radiation and beam scanning enabled was proposed [3], and the most recent and detailed findings of this work are presented in this letter.

The antenna design has broadside radiation enabled by the addition of matching sections to the unit cell, which is a method that has been verified in microstrip technology [4], [5]. The antenna thus offers radiating performance comparable to composite right/left-handed (CRLH) LWAs such as those presented in [6], albeit with a narrower scan range, which have in recent years been recognized for their broadside-scanning capabilities. A fundamental difference between CRLH LWAs and periodic LWAs is the radiating mode of the CRLH LWA is the fundamental mode of the structure, while the periodic LWA radiates through the $n = -1$ space harmonic. The proposed antenna also differs functionally from the work in [6] by offering maximum radiation in the plane of the substrate. Other SIW-based LWA designs have exhibited wide scan ranges, however they exclude broadside radiation such as the quasi-uniform LWA in [7]. The antenna measurements exhibited a 32% impedance bandwidth within which a 10-dB gain over an 86° scan range ($-43°$ to $43°$) was obtained from 8.4 to 11.4 GHz (30%).

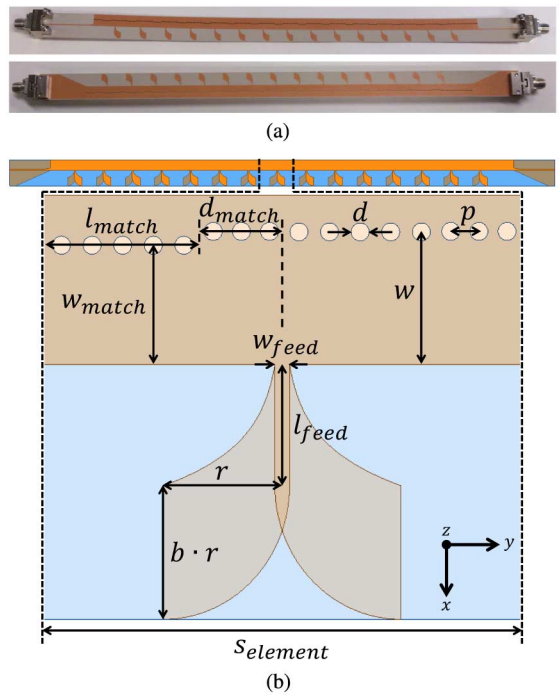

Fig. 1. HMSIW periodic LWA prototype and its geometry. (a) Antenna prototype (top and bottom perspectives). (b) Simulated full antenna and unit cell geometry (length units in millimeters): $p = 0.76, d = 0.508, w = 7.51, l_{\text{match}} = 4.31, w_{\text{match}} = 6.37, d_{\text{match}} = 2.34, w_{\text{feed}} = 0.42, l_{\text{feed}} = 3.42, r = 3.55, b = 1.06, s_{\text{element}} = 13.38, \epsilon_{rz} = 10.96, \epsilon_{rx} = \epsilon_{ry} = 13.3$.

II. Proposed Antenna

Periodic LWAs are generally realized through the introduction of periodic radiating perturbations to the guided mode of some structure such that the $n = -1$ Floquet mode becomes fast and radiating [8]. The guiding structure in this work is HMSIW, and the periodic radiating perturbations are antipodal tapered-slot antenna (ATSA) elements. Fig. 1 depicts the proposed antenna and its architecture. The antenna could have equivalently been viewed as a traveling wave array, however the weak loading of the radiating elements on the guided mode imply leaky-wave analysis is suitable [8].

Manuscript received May 09, 2014; revised June 23, 2014; accepted July 17, 2014. Date of publication July 25, 2014; date of current version August 04, 2014. This work was supported by NSERC.

The authors are with the Department of Electrical and Computer Engineering, Schulich School of Engineering, University of Calgary, Calgary, AB T2N 1N4, Canada (e-mail: rjhenry@ucalgary.ca; okoniews@ucalgary.ca).

Color versions of one or more of the figures in this letter are available online at http://ieeexplore.ieee.org.

Digital Object Identifier 10.1109/LAWP.2014.2341217

III. Antenna Design

A. Substrate, Antenna Excitation, and HMSIW Design

Assuming the antenna's fundamental-mode group velocity would be close to that of the guiding structure's, it can be shown that designing for a guided mode with a slower group velocity offered beam scanning over a narrower bandwidth [9]. This in turn relaxed the bandwidth constraints on the periodic radiating element design and increased the beam-scanning range to bandwidth ratio, as is usually preferred in high-performance radar applications [9]. A high-permittivity substrate was therefore chosen to reduce the fundamental-mode group velocity in the HMSIW. In particular, a Rogers RO3210 substrate with a design relative permittivity of 10.8 was used.

One problem encountered in the design of this antenna was that the substrate permittivity of the fabricated prototypes differed from the Rogers catalog design permittivity of 10.8 (which does not disclose the material's anisotropy). Simulations using the catalog permittivity resulted in an observed 3%–4% frequency shift from measurements. Upon consultation with Rogers, we changed the simulation relative permittivity to include axial anisotropy, with a z-directed component of 10.96 (which is more representative of the substrate at X-band frequencies), and xy-plane components of 13.3. This resulted in significantly improved convergence between measurements and simulations.

The structure used tapered microstrip for excitation and termination, the design of which is described in [10] and [11]. The microstrip ground plane had to be tapered to allow the introduction of the ATSA elements as shown in Fig. 1. The operating range of the antenna was chosen to be within 8–12 GHz, and so a simulated HMSIW cutoff of 6.2 GHz was deemed suitable. Parameters d, p, and w in Fig. 1(b) were chosen by modeling the HMSIW as an SIW with a width of $2w$ and using design equations from [12] for an equivalent X-band rectangular waveguide.

B. Radiating Element Design

The ATSA element was chosen for its bandwidth, observed weak perturbation of the fundamental HMSIW guided mode, as well as its radiating properties. The element geometry is shown in Fig. 1(b) and consists of a quarter-section of an ellipse with axial ratio b that is fed by an exponential taper intersecting w_{feed} and r at a distance l_{feed} from the open sidewall of the HMSIW. HFSS was used to optimize the unit cell in terms of the element parameters from 8 to 12 GHz as was outlined in [3].

C. Broadside Open Stopband Mitigation

The open stopband observed in periodic LWAs can be understood as a frequency band where the reflections from each periodic perturbation (radiating element) add constructively in the reverse direction resulting in a standing wave on the structure and a poor input impedance match. According to [4] and [5], the individual reflections can be minimized at the broadside frequency with the use of matching sections in order to ensure that the total reflection remains acceptably low. Matching was achieved by the addition of a reduced width section of HMSIW to the unit cell, defined by w_{match}, l_{match}, and d_{match} in Fig. 1(b). The matching section parameters were optimized in order to minimize the unit cell S_{11} at the desired broadside frequency (9.6 GHz). The addition of the matching section introduced a phase shift that needed to be removed in order to maintain 360° per unit cell (as required for broadside radiation). This was accomplished by adjusting the unit-cell HMSIW length after matching was acquired.

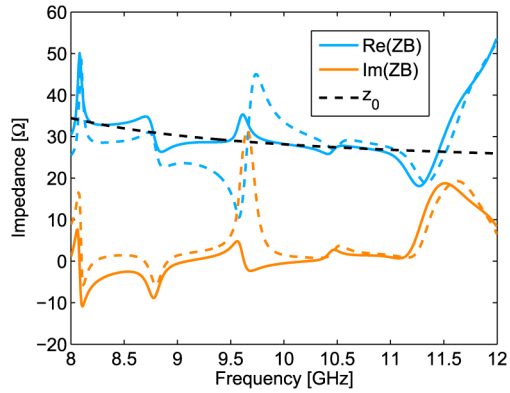

Fig. 2. Bloch impedance for the structure with (——) and without (– – –) matching sections.

The efficacy of this technique for open stopband mitigation was observed in the Bloch impedance of the periodic structure. Three unit cells were cascaded, both with and without matching sections, and simulated to acquire their transfer matrices. Multiple unit cells were cascaded to account for the mutual coupling of adjacent radiating elements. The transfer matrices were then processed as shown in [13] to calculate the Bloch impedance of the structures, which were compared to the HMSIW impedance (extracted from HFSS waveport solutions) as shown in Fig. 2.

For a periodic structure terminated with a real-valued impedance, maximum power transfer occurs when the source, load, and Bloch impedance are equal. Minimizing the unit cell S_{11} with the addition of a matching section was considered equivalent to matching the Bloch impedance to the real-valued HMSIW impedance (which was the source and load impedance of the periodic structure). Fig. 2 shows that the addition of the unit-cell matching section significantly improved the Bloch impedance matching to the waveguide impedance z_0 at the broadside frequency. Without the matching section, the Bloch impedance had a large reactive component at 9.6 GHz, which is indicative of stopband operation.

D. Prototype Fabrication

Five identical 15-element prototypes were fabricated using a photolithography-based process. Multiple prototypes were desired in anticipation of performance variations due to limitations of the process' drill placement accuracy. In particular, the ±3-mil accuracy was a concern considering minimum via spacing features of 10 mil exist in the design. Multiple prototypes have allowed us to observe the design sensitivity to this process limitation.

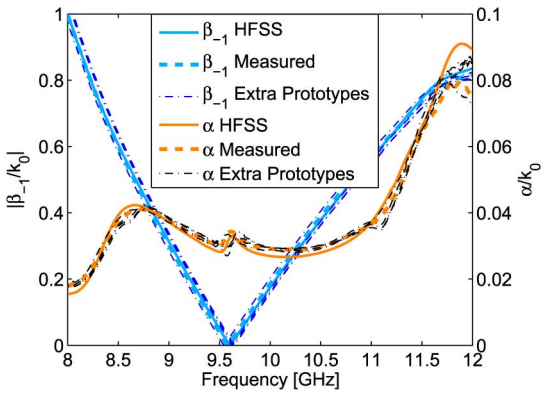

Fig. 3. Measured (five prototypes) and simulated normalized leaky wavenumbers k_{LW}.

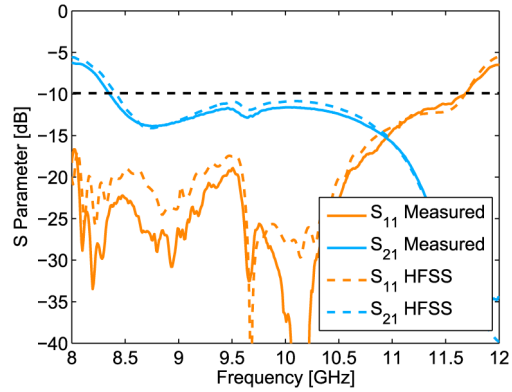

Fig. 4. S-parameters used to define impedance bandwidth.

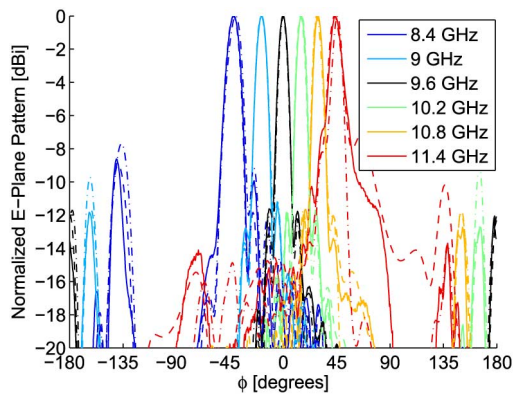

Fig. 5. Normalized copolarized E-plane (xy-plane) radiation pattern [dBi]: Measured (——), simulated (– – –), and theoretical (— · —·).

IV. Results

A. Leaky-Wave Analysis

The leaky wavenumber ($k_{\mathrm{LW}} = \beta_{-1} - j\alpha$, where β_{-1} is the phase constant of the $n = -1$ space harmonic and α is the mode attenuation coefficient) of the 15-element periodic structure was extracted from simulations and compared to the measured leaky wavenumbers of the five prototype antennas. In order to yield the best comparison, measurements and simulations both consisted of 15 cascaded unit cells. Results for the periodic structure were processed as in [13] in order to obtain the leaky wavenumber at each solution frequency. Measurements required the removal of connector effects using TRL calibration, and microstrip-to-HMSIW transitions were removed using HFSS simulations and standard deembedding techniques. The simulated and measured normalized leaky wavenumbers are shown in Fig. 3. One prototype was used subsequently for impedance and radiation pattern measurements (shown as β_{-1} Measured in Fig. 3).

The small differences between the simulated and measured leaky wavenumbers were likely due to the via placement accuracy of the fabrication process as well as measurement repeatability issues (cable movement as well as solder and connector differences). The prototypes were fabricated on the same panel, and so deviation in the substrate permittivity was probably an insignificant source of error. The leaky wavenumbers indicate broadside radiation (when $\beta_{-1} = 0$) at or near 9.6 GHz as anticipated by proper element spacing.

B. Impedance Bandwidth

The measured and simulated antenna S-parameters are presented in Fig. 4. In order to best represent the frequency range over which power was coupled to radiation rather than leaving the antenna ports, the impedance bandwidth should require both the return loss and insertion loss to be greater than 10 dB. By this definition, the antenna impedance bandwidth extended from 8.4 to 11.6 GHz (32%).

C. Radiation Pattern

Considering the coordinate system shown in Fig. 1(b), let us define a spherical coordinate system with the $+y$-direction as the zenith, ϕ as the polar angle, and θ as the azimuthal angle, both measured from $+x$. Theoretical, simulated, and measured normalized E-plane (xy-plane) radiation patterns for a sample of frequencies within the antenna impedance bandwidth are shown in Fig. 5. The antenna is linearly polarized in the ϕ-direction. Array theory and leaky wave theory were used in conjunction in order to predict the radiation pattern of the proposed antenna as is shown in [14]. Essentially the leaky wavenumber was used to calculate the phase and amplitude of each element excitation in order to compute an array factor. The array factor was then combined with the unit-cell element pattern to predict the radiation pattern of the antenna. The unit-cell element pattern was approximated in HFSS by simulating the proposed antenna with a single ATSA element at its center. The array factor computation for the 1-D array in three dimensions yields a cone shape beam that scans with frequency. Back radiation in the plane of the antenna ($|\phi| > 90°$) was reduced by the ATSA element pattern, resulting in a fan beam with maximum radiation in the $|\phi| < 90°$ region.

Although E-plane patterns were of main interest, simulated normalized H-plane patterns are also presented in Fig. 6 and correspond to the E-plane patterns in Fig. 5. The H-plane of the main beam was defined by the cone shape produced by the array factor of the antenna. At a particular frequency, $\theta = 0°$ corresponds to the main beam peak in the $|\phi| < 90°$ region, while $|\theta| = 180°$ corresponds to the back radiation peak in the $|\phi| > 90°$ region.

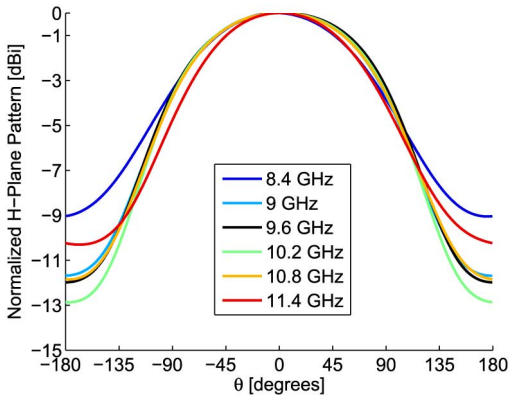

Fig. 6. Simulated normalized copolarized H-plane antenna radiation pattern [dBi].

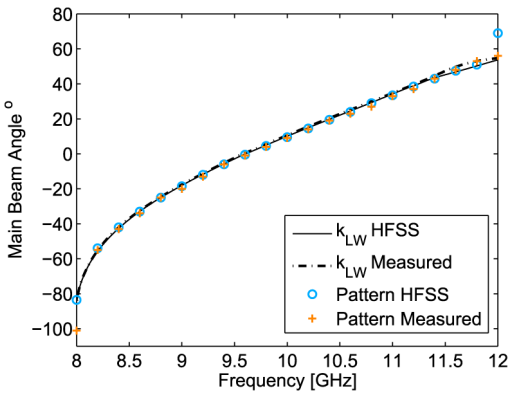

Fig. 7. Main beam scan angle.

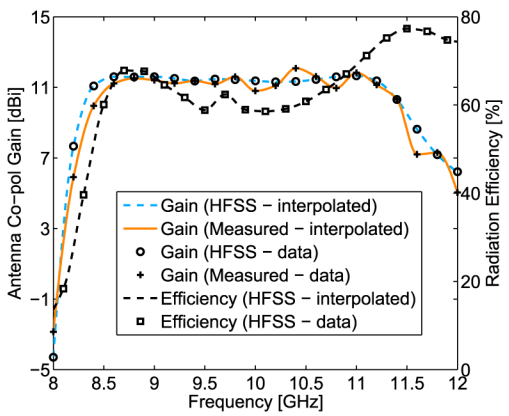

Fig. 8. Antenna gain and efficiency versus frequency.

The scanning behavior of the antenna is shown in Fig. 7 where the main beam angle (ϕ_{m}) has been reported as a function of frequency. Simulated and measured results are presented as well as theoretical results relying on the well-known relation $\phi_{\mathrm{m}} = \sin^{-1}(\frac{\beta_{-1}}{k_0})$. Both the simulated and measured β_{-1} values (from Fig. 3) were used in this relation and are presented.

D. Antenna Gain and Efficiency

The antenna gain, extracted from simulations and prototype measurements, is shown in Fig. 8. The simulated antenna efficiency is also presented and was between 52%–77% within the antenna impedance bandwidth. The efficiency calculation included power dissipated in the matched load as part of the accepted power. Reflected power was excluded from the calculation (as is customary).

V. Conclusion

The most recent results from the detailed study of a broadside-scanning HMSIW periodic LWA have been presented. The prototype antenna exhibited a 32% impedance bandwidth within which a 10-dB gain over an 86° scan range ($-43°$ to 43° including broadside) was obtained, thus offering comparable performance to many SIW-based CRLH LWAs. In the future, the X-band design should be scaled to mm-wave frequencies in order to evaluate whether or not it is indeed an acceptable design for these frequencies.

References

[1] M. Bozzi, A. Georgiadis, and K. Wu, "Review of substrate-integrated waveguide circuits and antennas," *Microw., Antennas Propag.*, vol. 5, no. 8, p. 909, 2011.

[2] D. Deslandes and K. Wu, "Integrated microstrip and rectangular waveguide in planar form," *IEEE Microw. Wireless Compon. Lett.*, vol. 11, no. 2, pp. 68–70, Feb. 2001.

[3] R. Henry and M. Okoniewski, "A new half mode substrate integrated waveguide leaky wave antenna," in *Proc. 8th EuCAP*, Apr. 2014, to be published.

[4] S. Paulotto, P. Baccarelli, F. Frezza, S. Member, and D. R. Jackson, "a novel technique for open-stopband suppression in 1-D periodic printed leaky-wave antennas," *IEEE Trans. Antennas Propag.*, vol. 57, no. 7, pp. 1894–1906, Jul. 2009.

[5] T. Cameron, A. Sutinjo, and M. Okoniewski, "A circularly polarized broadside scanning patch array," in *Proc. 4th EuCAP*, Apr. 2010, pp. 1–3.

[6] Y. Dong and T. Itoh, "Composite right/left-handed substrate integrated waveguide and half mode substrate integrated waveguide leaky-wave structures," *IEEE Trans. Antennas Propag.*, vol. 59, no. 3, pp. 767–775, Mar. 2011.

[7] J. Liu, D. Jackson, and Y. Long, "Substrate integrated waveguide (SIW) leaky-wave antenna with transverse slots," *IEEE Trans. Antennas Propag.*, vol. 60, no. 1, pp. 20–29, Jan 2012.

[8] A. Oliner and D. Jackson, *Antenna Engineering Handbook*. New York, NY, USA: McGraw-Hill, 1993, ch. 11.

[9] Q. Yang, Y. Zhang, and X. Zhang, "X-band composite right/left-handed leaky wave antenna with large beam scanning-range/bandwidth ratio," *Electron. Lett.*, vol. 48, no. 13, pp. 746–747, Jun. 2012.

[10] D. Deslandes, "Design equations for tapered microstrip-to-substrate integrated waveguide transitions," in *Proc. IEEE MTT-S Int. Microw. Symp.*, May 2010, p. 1.

[11] K. Lu, "An efficient method for analysis of arbitrary nonuniform transmission lines," *IEEE Trans. Microw. Theory Tech.*, vol. 45, no. 1, pp. 9–14, Jan. 1997.

[12] F. Xu and K. Wu, "Guided-wave and leakage characteristics of substrate integrated waveguide," *IEEE Trans. Microw. Theory Tech.*, vol. 53, no. 1, pp. 66–73, Jan. 2005.

[13] R. Collin, *Foundations for Microwave Engineering*, 2nd ed. New York, NY, USA: McGraw-Hill, 1992, ch. 8.

[14] C. Caloz and T. Itoh, "Array factor approach of leaky-wave antennas and application to 1-D/2-D composite right/left-handed (crlh) structures," *IEEE Microw. Wireless Compon. Lett.*, vol. 14, no. 6, pp. 274–276, Jun. 2004.